Monopole migration in ^{69,71,73}Cu observed from β decay of laser-ionized $^{68-74}$Ni

S. Franchoo,* M. Huyse, K. Kruglov, Y. Kudryavtsev, W. F. Mueller,† R. Raabe,‡ I. Reusen, P. Van Duppen,
J. Van Roosbroeck, L. Vermeeren, and A. Wöhr§

Instituut voor Kern- en Stralingsfysica, University of Leuven, B-3001 Leuven, Belgium

H. Grawe

Gesellschaft für Schwerionenforschung, D-64291 Darmstadt, Germany

K.-L. Kratz and B. Pfeiffer

Institut für Kernchemie, University of Mainz, D-55099 Mainz, Germany

W. B. Walters

Department of Chemistry, University of Maryland, College Park, Maryland 20742

The neutron-rich isotopes $^{68-74}$Ni have been produced at the LISOL facility in the fission of ^{238}U induced by a 30-MeV proton beam. They have been extracted selectively through resonant laser ionization and electromagnetic mass separation. Production rates have been deduced and deviate from theoretical predictions. The β decay of the isotopes has been investigated by means of β-γ and γ-γ spectroscopy. Half-lives have been determined for $^{68-74}$Ni, and the level scheme has been extended for ^{69}Cu and newly established for ^{71,73}Cu. The constructed schemes show an unexpected and sharp lowering of the $\pi f_{5/2}$ orbital with respect to the $\pi p_{3/2}$ ground state. This feature is ascribed to the monopole term of the residual proton-neutron interaction and is well reproduced by realistic shell-model calculations.

I. INTRODUCTION

The region of medium-mass neutron-rich nuclei around $Z=28$ and $40<N<50$ has been the subject of intensive experimental investigations in the last few years [1–5]. The reason for this interest is twofold. First of all, the evolution of the single-particle structures towards ^{78}Ni constitutes a test ground for the nuclear shell model. Although a doubly magic nature is propounded for this nucleus, it remains poorly understood to which extent the excess of neutron matter will act upon the nuclear properties. Probably most noticeably, Hartree-Fock-Bogoliubov (HFB) calculations foresee the displacement of shell gaps and a dilution of the spin-orbit interaction far from stability [6]. Recent theoretical work for the nickel isotopes ranges from straightforward Tamm-Dancoff-approximation (TDA) half-life estimates [7] to highly elaborate HFB+SkO′ predictions [8], while shell-model approaches allow the reproduction of various level structures with an ever growing degree of precision [9].

A second motivation is related to the astrophysical r process, which is the mechanism of rapid neutron capture by seed nuclei in explosive stellar environments [10]. While the detailed flow of this reaction network is difficult to establish, it is still supposed to follow a path among the neutron-rich nuclides dictated by the so-called waiting-point nuclei. In particular, it is generally suspected that the ^{78}Ni nucleus plays a privileged role. Therefore, if the predicted magicity around ^{78}Ni weakens or disappears, it may profoundly affect the stellar nucleosynthesis.

Amidst the former approaches endeavored to study the neutron-rich nickel isotopes, traditional deep-inelastic reactions of ^{76}Ge and ^{82}Se on natural tungsten have led to the half-life determination of ^{68}Ni [11] and unraveled the decay scheme of ^{69}Ni [12]. Quasielastic transfer on a ^{70}Zn target [13] or on ^{64}Ni projectiles [14] has indicated a possible neutron subshell closure in ^{68}Ni, the latter reaction equally deepening insight into the structure of ^{69}Cu [15]. Renewed experiments on multiproton transfer from ^{76}Ge have showed the existence of microsecond isomers in ^{70}Ni and ^{69,71}Cu [3,15,16].

Nevertheless, in spite of its success near the brink of stability, the technique suffers from sharply dropping reaction yields for exotic nuclei. On-line mass separation, on the other hand, is generally limited by the difficult and slow extraction of nickel from conventional plasma or surface-ionization sources. While the half-life measurement of ^{68}Ni could still be achieved by means of a hot-cavity ion source at the on-line mass separator of GSI-Darmstadt [17], at ISOLDE-Geneva the release time surpasses several hundreds of seconds [18], inhibiting spectroscopy beyond ^{69}Ni.

Almost all experiments so far aiming at neutron-rich nickel isotopes have therefore been performed at fragment separators. The first identification of $^{70-74}$Ni and lifetime determination of $^{71-74}$Ni have been carried out through thermal-neutron-induced fission of ^{235}U and ^{239}Pu at the Lohengrin recoil spectrometer of ILL-Grenoble [19]. The fragmentation of ^{86}Kr at the LISE-3 separator of GANIL-Caen

————

*Present address: CERN, CH-1211 Geneva 23, Switzerland.

†Present address: NSCL, Michigan State University, East Lansing, Michigan 48824.

‡Present address: CEA Saclay, F-91191 Gif-sur-Yvette Cedex, France.

§Present address: Physics Department, University of Oxford, Oxford OX1 3PU, United Kingdom.

has allowed for the investigation of additional microsecond isomers in [67-70]Ni, [69,71-72]Cu [1], and [78]Zn [5]. The same reaction at higher beam energies has enabled the measurement of the half-life of [73-76]Ni at the FRS device of GSI-Darmstadt [20]. Attempts to reach exotic nickel and copper by fragmentation of [76]Ge have been undertaken at MSU-East Lansing [21,22]. Recently, much effort has been devoted to relativistic fission of the incoming projectile in inverse kinematics. The pioneering work at the FRS machine has been credited with the first identification of [77]Ni and the long-sought [78]Ni [23].

The development of a laser ion source at LISOL-Leuven [24] has brought a sharp turn in this situation. Opting for charged-particle-induced fission reactions in combination with a highly advanced ion-guide and laser technology, we have been able to surmount the restrictions of multinucleon transfer reactions as well as the shortcomings of earlier ISOL ion sources. Producing remarkably pure samples of the isotopes of interest, β-decay studies could be performed by means of β-γ and γ-γ spectroscopy. As a result of the selectivity of the Gamow-Teller operator, it has provided us with a unique way to probe for specific single-particle structures. The decay of [69,71,73]Ni has yielded evidence for the monopole migration of the $\pi 1 f_{5/2}$ orbital [2], while the strength of the $N = 40$ subshell closure around the semimagic nucleus [68]Ni has been carefully explored [4].

In this paper we report on the β decay of [68-74]Ni. In the following section we turn to the setup of the experiments carried out at the LISOL separator. The identification procedure for the newly discovered γ rays is described and the measured half-lives are compiled. Next we extract the production rates for [68-74]Ni and compare these to theoretical predictions. The efficiency and the selectivity of the laser ion source are deduced. In the subsequent sections we present the decay schemes obtained for [69,71,73]Cu. We investigate the evolution of single-particle structures and discuss some recently developed theoretical approaches.

II. EXPERIMENTAL SETUP

The neutron-rich nickel isotopes are produced in proton-induced fission of [238]U. The 30-MeV proton beam with a typical dc intensity of 10 μA is delivered by the $K = 110$ cyclotron at Louvain-la-Neuve. It crosses a 5-μm Havar window before entering the ion source, where it impinges on two foils of natural uranium with a thickness of 10 mg/cm^2. In order to maximize the production rate, the targets are tilted to an angle of 20° with respect to the beam axis. It is estimated that fission fragments in the mass region $A \approx 70$ carry away about 120 MeV, which results in a fraction of 30% of recoils that emerge from the targets towards the interior of the ion source.

The inner volume of the ion source measures $5 \times 2 \times 2$ cm^3. Inside the source a continuous flow of argon buffer gas is maintained at a pressure of 500 mbar. The gas is purified to the part-per-10^9 level. About 30% of the reaction products is stopped and thermalized by collisions with the argon atoms. The recoiling ions reside in the gas cell for several milliseconds, long enough to allow for their neutral-

ization. An important role herein is played by the available plasma electrons, created by the impact of the cyclotron beam on the buffer gas.

The radioactive atoms are guided downstream by the gas flow into the pathway of a laser system. At this point resonant photoionization takes place, enabling for the exclusive selection of the nickel isotopes present. The removal of an electron proceeds in two steps. A first laser photon of 232.00 nm wavelength excites the atom from the $^3F_4$ ground state to the $^3G_5$ intermediate state. A second photon of 537.84 nm lifts the atom into an autoionizing state.

The photons are delivered by two dye lasers. For the first step, a frequency-doubled second harmonic is generated. The dye lasers are pumped by two synchronized excimer XeCl lasers that emit ultraviolet photons of 308 nm wavelength. The laser light irradiates the gas cell along its longitudinal axis at a repetition rate of 200 Hz, fast enough to ensure that the majority of the atoms cross the laser paths at least once. The pulse width measures 15 ns, the diameter of the laser beams about 5 mm. The energy per pulse amounts to 0.3 and 3 mJ for the first and second steps respectively.

After 200–300 ms, most of the ions are evacuated from the source through an exit hole of 0.5 mm diameter. The large pressure gradients turn the gas flow into a rapidly expanding shock wave. While the neutral atoms are being pumped away, the ions of interest are directed by means of a potential difference of 250 V towards a sextupole ion guide (SPIG) [25]. This structure allows for the smooth transition from the high-pressure area of the gas cell to the low-pressure zone of the mass separator.

The SPIG consists of six metallic rods cylindrically mounted behind the exit hole of the ion source. The length of the rods measures 124 mm, and the inner diameter of the structure equals 2.5 mm. The distance from the exit hole of the source to the entrance of the SPIG is fixed at 2.5 mm. An oscillating voltage with a frequency of 4.7 MHz and an amplitude of 150 V is applied on the device such that every other rod is at all times in antiphase with its neighbors. While the electromagnetic field radially confines the radioactive ions, the remnants of the neutral gas jet escape through the open space between the rods and are likewise pumped away. The frequent collisions with the gas atoms during the first few millimeters inside the SPIG effectively cool the ions such that on leaving the cylinder the kinetic-energy spread of the beam on the symmetry axis is narrowed to less than 1 eV.

The beam is injected into the mass separator, consisting of a 55° magnet with a radius of 1.5 m. The mass resolving power, given by the ratio of the separated mass M to the full width at half maximum of the mass peak in the focal plane ΔM, reaches 1450. Prior to the implementation of the SPIG, the mass resolution amounted to only 300.

The mass-separated nickel ions are implanted in a Mylar tape of 6 mm width. The tape tube is surrounded by two high-purity germanium detectors with a relative efficiency of 70% and 75%, respectively. Both detectors are positioned opposite each other at 1 mm from the implantation chamber, while in between a plastic ΔE scintillator with a thickness of 1 mm and a surface area of 12×50 mm^2 is sandwiched. The energy spectra of the germanium detectors are cali-

brated with off-line radioactive sources of ^{152}Eu and ^{60}Co before and after the experimental runs. In most cases a parabolic dependence of the energy on the channel number is observed and quadratic fits are performed to yield reliable results. Extrapolation of the fit beyond the last calibration point at 1408 keV induces a systematic error, which is accounted for by the larger error bars. This refined treatment has induced some differences with respect to the energy values quoted in Ref. [2], notably for ^{71}Cu.

The efficiencies of the detectors are determined by means of intensity-calibrated radioactive sources of ^{154}Eu, on-line radioactive sources of ^{98}Y, ^{98}Nb, and ^{144}Ba, as well as the computer code GEANT [26]. The latter explicitly takes into account the scattering of β particles into the germanium crystals, which is caused by the proximity of the various detectors to the metal frame of the tape system. Since a reliable off-line reconstruction of the actual experimental conditions is often difficult to realize, the efficiencies computed by GEANT are further adopted as final values, while the efficiency results derived from the calibration sources serve as a confirmation.

The detection setup is shielded from external γ radiation by 5-cm-thick lead bricks. To prevent fission neutrons from penetrating into the detectors, the construction is surrounded by 10 cm of borax blocks and covered by 20 cm of polyethylene grains in plastic bags. Active background suppression is achieved by applying β-γ and γ-γ coincidence conditions on the data acquisition as well as the implementation of a pulsed time structure.

Even when the laser light is switched off, a small fraction of the reaction products escapes from the gas cell as ions in a 1^+ or 2^+ charge state, giving rise to a nonresonant signal. In order to reduce the background radiation originating from the decay of these ions, a cyclic time structure is implemented. So the proton beam is triggered for a span of 250 ms, while transmission through the SPIG is inhibited. Hereafter 250 ms follow during which protons are no longer accelerated. The SPIG voltage is switched on 5 ms after the cyclotron bombardment has stopped, avoiding too large a space charge to build up that might eventually block the SPIG. Current is released from the ion source for 245 ms, after which the SPIG field is disabled once more and the cyclotron beam resumes. It has been determined that 250 ms correspond to the mean evacuation time of the gas cell.

Moreover, an asymmetric macrostructure is superimposed onto the described microstructure. Its first part consists of the previous microcycle repeated for an integer number of times. A second half is appended during which the cyclotron is tuned down and the SPIG field turned off. At the end of the macrocycle, the Mylar tape at the detection station is reeled in over a couple of centimeters. It removes the radioactivity of the remaining decay products, before the macrocycle starts over again. The resulting time structure entails that the measurements can be divided in a macrocycle growing-in period, marked by a high background of fission neutrons produced during beam irradiation of the target, and an almost noise-free decay interval. Since the half-lives of the parent nuclei are to be deduced out of the time behavior of the emitted γ rays, the growing-in period is generally

TABLE I. Investigated mass A, macrocycle on-off period, total measurement time Δt, and beam-pulse current I on and off resonance.

		On resonance		Off resonance	
A	Cycle (s/s)	Δt	I (μA)	Δt	I (μA)
68	40/120	25 h 03 min	5.6	6 h 08 min	6.2
69	6/10	9 h 01 min	6.1	—	—
70	24/40	5 h 24 min	10.1	2 h 00 min	10.3
71	6/10	35 h 09 min	6.1	7 h 09 min	2.5
72	6/10	11 h 52 min	6.4	3 h 20 min	6.0
73	3/5	28 h 39 min	8.2	7 h 05 min	12.0
74	3/5	13 h 12 min	8.4	3 h 44 min	6.2

chosen to match two or three lifetimes and the decay five to six.

The applied macrocycles for the nickel isotopes investigated are listed in Table I. Also included are the total measurement times Δt and the cyclotron beam-pulse currents I, the latter defined as the currents measured when switching off the pulsation. Both quantities appear for the runs with and without laser irradiation of the gas cell. Note that at mass 69, only resonant data were collected. At mass 71, the off-resonance statistics stem from an earlier preliminary experiment at LISOL and have been published elsewhere [27].

The β-gated γ spectra collected at mass 69, 71, and 73 are plotted in Figs. 1–3. For mass 73 the data on resonance, with laser light present in the gas cell, and the off-resonance counts, accumulated without laser light shining into the cell,
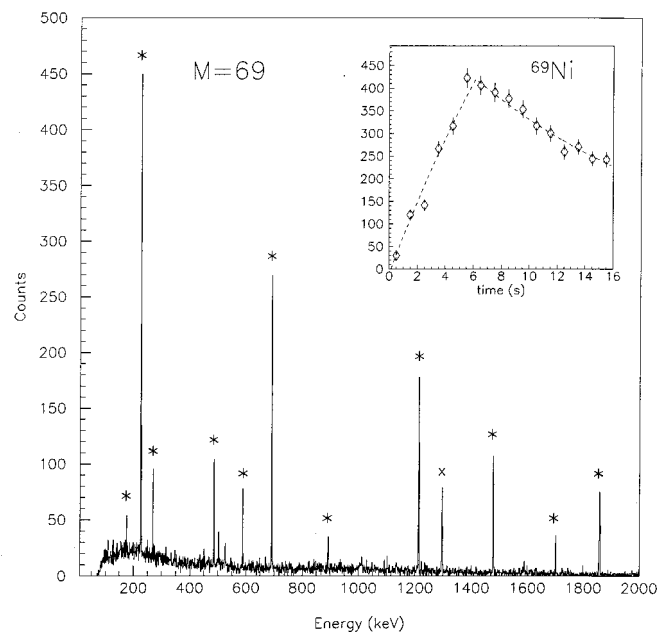

FIG. 1. Beta-gated γ spectrum on resonance for mass 69. The integrated proton beam dose was 3.7×10^4 μC. The rays belonging to the decay of ^{69}Ni are marked with an asterisk, to the decay of ^{69}Ni^m with a cross. The inset shows the time evolution of the γ intensity attributed to the decay of ^{69}Ni, with an exponential fit drawn through the data.
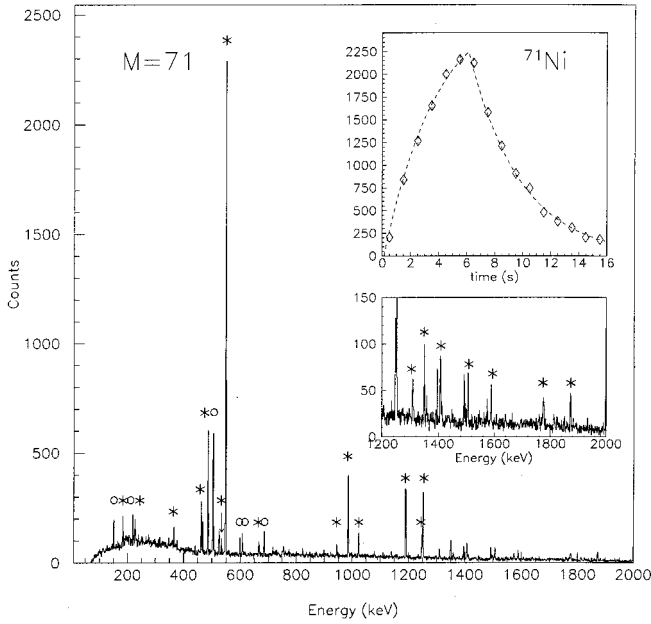
FIG. 2. Beta-gated γ spectrum on resonance for mass 71. The integrated proton beam dose was 1.4×10^5 μC. The rays belonging to the decay of ^{71}Ni are marked with an asterisk, to the decay of ^{71}Cu with a circle. The high-energy part of the spectrum is enlarged in the lower inset. The upper inset shows the time evolution of the γ intensity attributed to the decay of ^{71}Ni, with an exponential fit drawn through the data.
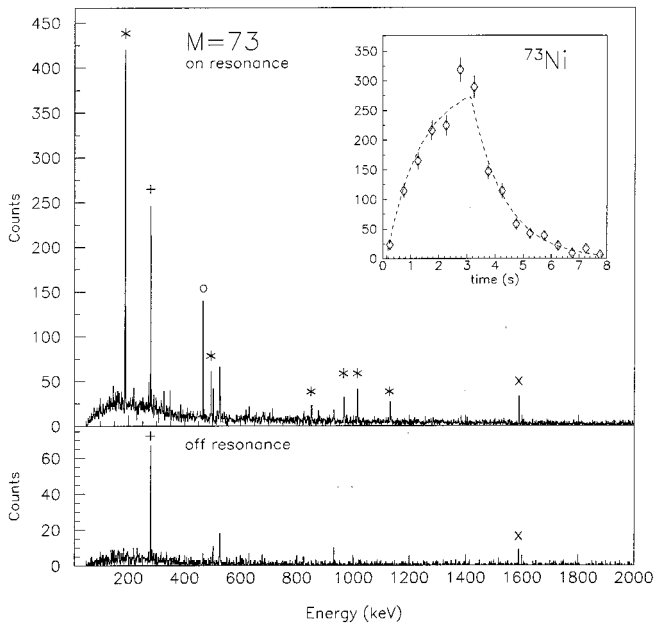

FIG. 3. Beta-gated γ spectra on and off resonance for mass 73. The integrated proton beam dose was 1.6×10^5 μC and 5.7×10^4 μC, respectively. The off-resonance spectrum has been multiplied by 2.8 to account for this difference. The rays belonging to the decay of ^{73}Ni are marked with an asterisk, to the decay of ^{73}Cu with a circle. The straight cross refers to background arising from ^{146}La^{2+}, the oblique to long-lived ^{140}La contamination. The inset shows the time evolution of the γ intensity attributed to the decay of ^{73}Ni, with an exponential fit drawn through the data.

are drawn. The off-resonance spectrum is multiplied by an appropriate scaling factor to account for the difference in beam dose with the on-resonance statistics. Since the γ lines belonging to the decay of copper that are visible in the on-resonance spectra are nearly completely suppressed off resonance, the copper contribution must originate from the nuclear decay of the laser-ionized nickel nuclei. This proves the resonant signal coming out of the source chiefly consists of nickel and does not contain directly produced copper, which in turn ensures the selectivity of the ion source.

III. HALF-LIFE DETERMINATION

The identification of γ rays proceeds in several steps. First of all, peaks that are present in the on-resonance β-gated γ spectra and not in their off-resonance counterparts in principle can only result from photoionization in the reaction chamber. Hence it restricts the possible assignments to the decay of nickel or its daughters. A second criterion follows from the time behavior of the γ activity. In particular, the time pattern of a daughter nucleus is unambiguously delayed with respect to that of a directly produced mother. A third procedure results from the analysis of the recorded γ-γ coincidences. Weaker peaks for which the coincidence condition is fulfilled can at this point be assigned to the decay of nickel.

At mass 70 a little more caution is required to distinguish the mother from the daughter nucleus. The lifetime of ^{70}Cu is found to be shorter than that of ^{70}Ni, which renders the time curves of both isobars rather similar. However, systematics of the neighboring even-even zinc nuclei show that there is no level in ^{70}Zn lower than the first excited 2^+ state at 885 keV [28]. Unknown resonant and short-lived γ peaks

TABLE II. Gamma-ray energies E and relative intensities $\dagger_\gamma$ detected in the decay of ^{69}Ni. The ray marked with an asterisk stems from the decay of ^{69}Ni^m.

E (keV)	$\dagger_\gamma$ (%)
104.1(2)	2.4(5)
154.1(1)	4.5(6)
205.1(1)	61.5(21)
231.4(10)	0.9(3)
249.1(1)	9.5(17)
262.8(2)	0.1(2)
470.7(1)	28.0(16)
574.9(1)	27.2(15)
584.8(3)	0.5(5)
680.5(1)	94.6(22)
780.8(3)	1.2(6)
1089.3(4)	2.0(8)
1213.5(1)	100.0
*1297.9(1)	—
1389.5(5)	3.3(8)
1483.6(4)	78.6(28)
1711.9(6)	33.9(21)
1872.3(8)	94.6(32)

TABLE III. Gamma-ray energies E and relative intensities $\dagger_\gamma$ detected in the decay of ^{71}Ni.

E (keV)	$\dagger_\gamma$ (%)
161.4(1)	2.9(6)
206.1(1)	2.5(6)
348.1(1)	3.2(6)
446.9(1)	9.7(7)
472.0(1)	22.5(9)
520.2(1)	2.7(6)
534.4(1)	100.0
655.1(1)	3.2(6)
705.7(2)	1.8(6)
744.7(1)	2.2(6)
939.5(2)	4.6(7)
981.3(1)	32.1(10)
1019.0(3)	8.2(7)
1138.9(2)	2.5(8)
1189.5(1)	33.4(10)
1248.2(1)	11.7(13)
1251.7(1)	36.1(10)
1297.8(2)	1.4(5)
1311.3(1)	4.9(10)
1352.6(1)	9.8(9)
1410.4(1)	10.0(10)
1497.1(2)	6.6(10)
1581.0(4)	3.6(8)
1885.9(8)	7.7(9)
2017.0(10)	36.7(14)

in this mass chain with an energy less than 885 keV will therefore not originate from the decay of ^{70}Cu and can safely be attributed to the decay of ^{70}Ni. It is checked that these lines are not coincident with the 885-keV ray or other high-energy transitions providing a possible connection to the zinc ground state. Progressing recursively, we fit the half-life deduced from this prescription through the remaining γ peaks. Those cases for which agreement is manifest are equally assigned to the decay of ^{70}Ni.

Contaminating long-lived γ lines appearing in the

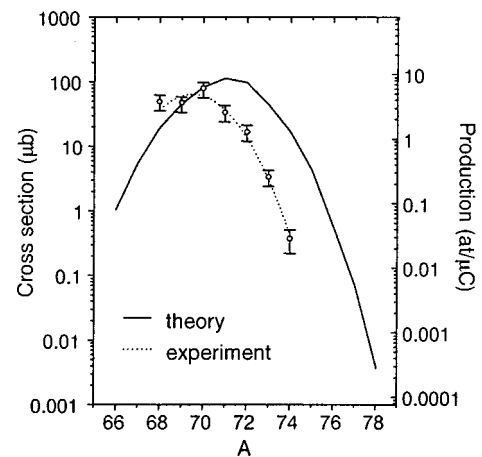TABLE IV. Gamma-ray energies E and relative intensities $\dagger_\gamma$ detected in the decay of ^{73}Ni.

E (keV)	$\dagger_\gamma$ (%)
166.1(1)	100.0
478.9(1)	27.2(24)
676.9(7)	5.0(11)
844.2(2)	29.3(33)
961.2(2)	33.3(40)
1010.0(2)	39.9(41)
1088.2(6)	3.8(11)
1131.9(2)	28.8(28)
1542.2(10)	5.0(13)
1995.5(14)	6.8(18)

TABLE V. Measured production rates $\mathcal{P}$ and half-lives $t_{1/2}$ for $^{68-74}$Ni. Literature values stem from [11,12,19,20].

	$\mathcal{P}$ (at/μC)	$t_{1/2}$	$t_{1/2}$, literature
^{68}Ni	3.6(7)	29(2) s	19^{+3}_{-6} s
^{69}Ni	4.3(8)	11.2(9) s	11.4(3) s
^{70}Ni	6(1)	6.0(3) s	—
^{71}Ni	3.0(6)	2.56(3) s	1.9(4) s
^{72}Ni	1.1(2)	1.57(5) s	2.1(3) s
^{73}Ni	0.26(6)	0.84(3) s	0.6(1) s
^{74}Ni	0.034(9)	0.9(2) s	0.5(2) s

collected data chiefly stem from the decay of barium and lanthanum isotopes, two elements that are situated near the maximum of the fission cross section. Because of their overwhelming production rate, a substantial fraction succeeds to escape from the ion source in a 2^+ charge state. Separated at the same A/Q ratio as the neutron-rich nickel, they pop up in the spectra at masses 72 and 73. In addition, the ^{140}Ba and ^{140}La isotopes with half-lives of 12.75 d and 40.27 h, respectively, are discerned at several masses throughout the experiment.

In Tables II–IV we print a compilation of the registered γ transitions. The relative intensities $\dagger_\gamma$ are expressed in percent normalized to the strongest ray. In Table V we list the experimental half-lives obtained from fitting the time behavior of the identified γ rays, along with literature values. The fluctuations out of the 1σ limit between our measurements and the published figures are manifold. Except for ^{69}Ni and ^{74}Ni, the present error bars are smaller by a factor of 2–10. At mass 68, the former half-life of 19^{+3}_{-6} s was deduced from a multinucleon-transfer experiment at the mass separator of GSI-Darmstadt and had only been reported in conference proceedings [11]. The lifetime of ^{70}Ni is measured in the current work for the first time. For $^{71-74}$Ni the previously known values were determined by means of a correlation technique [19,20]. For a further discussion of the presented

FIG. 4. Experimental production rates for $^{68-74}$Ni in 30-MeV proton-induced fission of ^{238}U compared to cross-section calculations from [30].

half-lifes and a comparison with theoretical predictions we refer to earlier publications [2,8].

IV. CROSS SECTIONS

The independent production yields for the heavy nickel isotopes expressed per unit of charge of the impinging beam are found from the count rates of the strongest γ transitions that have been assigned to the respective decay patterns. However, the relevant absolute γ intensities I_γ are available from the existing literature for the decay of ^{69}Ni only [28] and from our own measurements during an earlier exploratory experiment at the LISOL laser ion source for the particular case of ^{71}Ni [27]. For the remaining masses, we calculate the production rates from the γ quanta emitted by the daughter nuclei.

The γ branchings in the copper daughter decay can be retrieved from the literature for $^{68-70,72}$Cu [28]. For the 449.8(2)-keV ray in the decay of ^{73}Cu, a value of $I_\gamma = 43(12)\%$ has been measured by Huhta *et al.* [21], while the intensity of the 605.7(1)-keV transition following the decay of ^{74}Cu has been fixed by Fogelberg at $I_\gamma = 79(15)\%$ [29].

The production rates for $^{68-74}$Ni are presented in Table V and plotted in Fig. 4. Since the yield curve has been measured over a range of more than two orders of magnitude, an accurate and reliable Gaussian fit through the data points is possible. The mean we find to be situated at mass 69.4(3). The width, which we take as twice the standard deviation, equals 2.9(3) mass units.

A theoretical model for production cross sections in proton-induced fission has been proposed by Huhta *et al.* and satisfactory agreement has been reached in asymmetric fission for zinc to germanium [30]. However, the quality of the concerned data deteriorates for the lighter copper and nickel elements, which is likely due to uncertainties in the adopted branching ratios that complicated the extraction of independent yields out of the cumulative rates. Note that for the experiments at LISOL this problem does not exist because of the isotopic purity of the generated sample.

The calculations by Huhta *et al.* for the nickel cross sections locate the Gaussian mean at mass 71.0 and define a width amounting to 3.0 mass units. Confronting this with the present measurements, we encounter a shift of the experimental mean mass with 1.6 units towards stability. The measured width is consistent within the error bars. The ratio of the areas of the theoretical and experimental curves, 400 μb to 19 atoms/μC, results in a normalization factor of 21 μb μC.

Recently a saddle-point model for fission has been developed by Benlliure *et al.* [31]. Although the width is slightly overestimated, they correctly reproduce the position of the maximum.

The efficiency of the laser ion source is contained in the proportionality factor of the deduced production rates and the theoretical cross sections from Huhta *et al.*, the latter shifted by 1.6 mass units closer to β stability. Since the projectile is not appreciably slowed down in the thin target foils, the eventual energy dependence can be omitted. If we

isolate a factor of 30% for the produced ions that recoil out of the target and a further share of 30% for those that are stopped in the buffer gas, then by the efficiency of the laser ion source we account for all remaining processes the particles undergo inside the source until the exit of the SPIG. For this quantity we obtain a value of 0.05%.

The limited efficiency of the source is to be ascribed to several processes. Chemical bonds of the neutralized atoms with molecular impurities present in the gas cloud and neutralization into a metastable state different from the ground state prevent laser ionization. Further losses stem from diffusion to the walls of the gas cell and deposition onto its surfaces. Part of the laser-ionized particles are also neutralized anew or appear in side bands as $Ni(H_2O)_n^+$ ligands. A fair share of the latter can be dissociated by applying a small acceleration voltage of 250 V between the exit hole of the gas cell and the entrance of the SPIG, significantly reducing the intensity of sidebands in the mass spectrum.

The ion-source performance for fission reactions can be compared with the efficiency value of 3.7% achieved with the IGLIS source for fusion-evaporation reactions [32]. The conditions created by the specific reaction inside the source thus bear a definite influence on the thermalization and neutralization processes. Also, the rather small efficiency for fission implies the inherent potential for future improvements to the setup.

The selectivity of the laser ion source is a measure of the purity of the produced sample and is defined as the ratio of the number of counts in a specific γ peak belonging to nickel with laser irradiation of the gas cell relative to the number of counts without laser irradiation. After appropriately correcting the denominator for the difference in beam dose, a selectivity of 30 is calculated. The finite result is due to recoil products that escape neutralization as well as neutralized fragments that are reionized by radioactivity and fast electrons crossing the cell. The plasma provoked by the cyclotron beam is comparatively cold and is expected to contribute little. We point out that the selectivity of the IGLIS source for fusion-evaporation reactions reaches 400 [32].

V. COMPARISON WITH OTHER TECHNIQUES

Next to proton-induced fission, the reaction mechanisms available at present with which neutron-rich nuclei have been attained include fission induced by thermal neutrons [19], fragmentation [20], and projectile fission [23]. While the intrinsic production probability for these techniques is expressed by the cross section σ, the technical feasibility is comprised in the luminosity $\mathcal{L}$, the latter expressed as the product of the primary beam intensity and the target thickness. The production rate in atoms per second, denoted by P, can be written as

$$P = \sigma \varepsilon \mathcal{L},$$

with ε the efficiency of the source.

Table VI lists these quantities for the selected experiments. The respective efficiencies boil down to a collection range of 5×10^{-7} for thermal-neutron fission [19], a trans-

TABLE VI. Expected cross sections σ, efficiencies ε, luminosities $\mathcal{L}$, and production rates P for ^{78}Ni. Extrapolated values are printed in italics. Data from [19,20,23] and this work.

	σ (nb)	ε (%)	$\mathcal{L}$ (s^{-1}cm^{-2})	P (day^{-1})
n_{th} + ^{235}U	*20*	5×10^{-7}	2×10^{33}	2
500 MeV/nucleon ^{86}Kr+^{9}Be	*0.001*	35	4×10^{31}	0.9
750 MeV/nucleon ^{238}U+^{9}Be	0.3	1.6	1×10^{30}	0.5
30 MeV p+^{238}U	*0.01*	0.005	7×10^{33}	0.3

mission ratio of 35% for fragmentation [20], and a smaller 1.6% efficiency for relativistic fission [23]. The value for proton-induced fission from this work equals 0.05%, which is to be multiplied by the earlier mentioned factors of 30% for the fraction of reaction products that recoil out of the target and 30% for those ions that are stopped in the buffer gas.

As may be read from Table VI the lower intensities for heavy-ion beams are compensated for by the use of thicker targets. Reversely, the intense neutron fluxes or proton beams always impinge on thin target foils to facilitate the recoil of the produced species. Therefore, in all four cases the luminosities are roughly equal.

Out of the compiled cross-section predictions as well as the measured result for the case of projectile fission, we can calculate the corresponding production rates for ^{78}Ni. The cross section for ^{78}Ni in proton-induced fission we extrapolate from the Gaussian curve premised by Huhta *et al.* [30]. Shifted by the discussed 1.6 mass units towards β stability, this returns 10 pb. The projected production rate turns out to be 0.3 atoms per day. This is comparable with the achieved rate of 0.5 atoms per day for projectile fission of ^{238}U and the prospect of 0.9 atoms per day for fragmentation of for instance a ^{86}Kr beam. The expected 2 events per day for thermal-neutron induced fission are to be considered with some reserve due to the increasing complications in isotope identification far from stability.

With the current setup at LISOL, a production rate for ^{78}Ni of 0.3 atoms per day renders an experiment unfeasible. However, since the efficiency of the IGLIS source amounts to 0.05% only, the potential for further advance is vast and improvements in the efficiency and selectivity are continuously under development. Recently a thin aluminum window has been inserted in the gas cell to separate the reaction and thermalization zones, increasing the production yields by a factor of 5. Active suppression of atomic contaminations by controlled mixing of molecular impurities into the buffer gas is currently being evaluated.

Another aspect of the present setup which is susceptible of improvement is the detection efficiency. New scintillator detectors that meanwhile have been constructed raise the β efficiency from 30% to 60%. Installation of part of the Miniball cluster detector array [33] will enhance the γ efficiency in the foreseeable future by an additional factor of 5. The possibility of γ-ray tracking with these detectors is also being investigated. Such a technique would allow to distinguish full-energy γ rays from Compton events, the latter still accounting for the major source of background.

An upgrade of the production rate by a factor of 5 and the

detection efficiency by a factor of 10 readily suffices to extend the β decay studies to $^{75-76}$Ni already in the near future. Next to this, it remains to be stressed that the most important asset of the IGLIS source at LISOL resides in the successful delivery of a sample pure enough to perform β-decay spectroscopy.
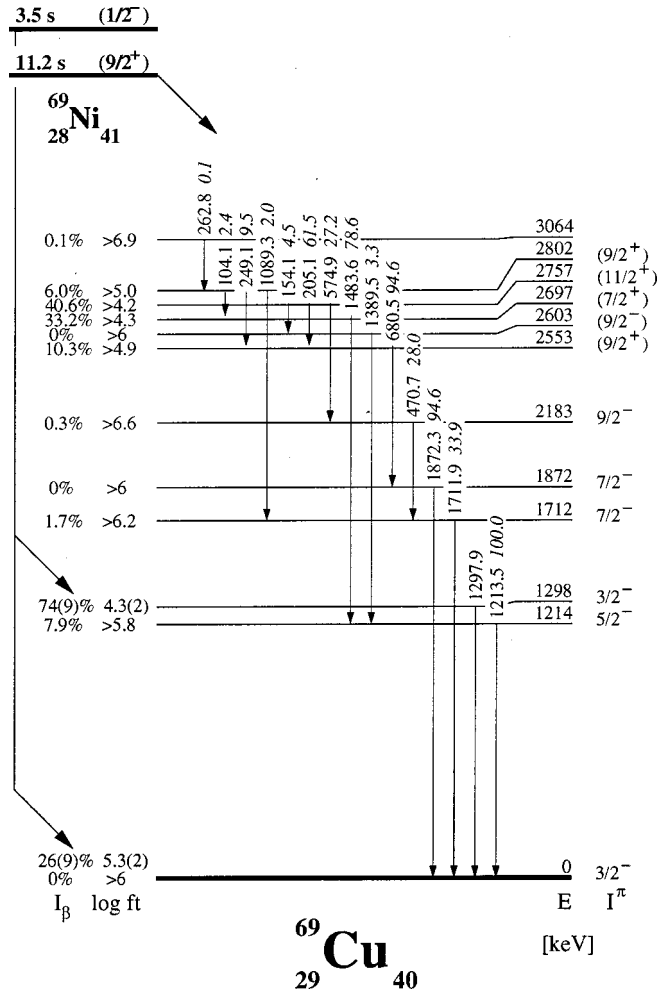
VI. LEVEL SCHEMES

The construction of the level schemes is based on the analysis of the recorded γ-γ coincidences by means of the Ritz principle and the relative intensities of the various rays. In order to distinguish an artificially induced sum peak from an actual transition, we estimate the probability for the summing of two intense photopeaks from the product of the γ efficiencies involved. The detected sum lines are removed from the level scheme.

In order to calculate log ft values the necessary Q_β energies are adopted from the literature [34]. Appropriate assumptions for the ground-state β branch will be propounded below. One should at all times keep in mind that the quoted log ft values are to be considered as lower limits. Because of the limited statistics and since the γ detection efficiency severely decreases for high-energy transitions, we might have missed part of the γ activity arising from levels above 2 MeV. This circumstance biases the β intensities to the various levels and leads to a reduction of the log ft results.

A. ^{69}Cu

The deduced level scheme for ^{69}Cu is reproduced in Fig. 5 and is consistent with the literature [12,15,16]. However, the 574.9(1)-keV ray we place on top of the 470.7(1)-keV line, in agreement with the transfer experiments [15,16] but disproving the previous β-decay results [12]. For some of the levels and transitions the energy values we obtain differ with up to 2.6 keV from earlier published values, in particular at the higher energies. The reported 183.2(5)-keV line, for which one would expect $\dagger_\gamma=10(1)$, has not been detected in this work.

A couple of new transitions have been discovered and placed, resulting in additional levels at 1298 and 3064 keV. Three weak rays at 231(1), 584.8(3), and 780.8(3) keV with respectively $\dagger_\gamma=0.9(3)$, $\dagger_\gamma\lesssim1.0$, and $\dagger_\gamma=1.2(6)$ could not be incorporated. The 154.1-keV ray has been put on top of the 1389.5-keV transition, giving rise to an intermediate level at 2603 keV. The reversed order would lead to a level at a lower energy, for which we shall show below no theoretical justification would be available. The intensity mismatch in-

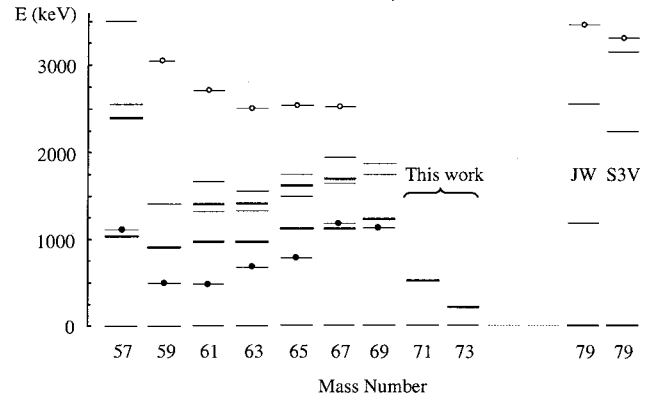FIG. 5. Decay scheme of ^{69}Ni. For discussion, see text.

FIG. 6. Systematics of the odd copper isotopes. Thick lines refer to levels with spin and parity $5/2^-$, those connected with a dashed line to $3/2^-$, those with a solid circle to $1/2^-$, those with an open circle to $9/2^+$. Theoretical levels in ^{79}Cu marked JW are taken from [42], those S3V from [37].

duced remains within the uncertainty limits.

A $3/2^-$ spin and parity has been observed in transfer reactions for the ground state of ^{69}Cu [35]. The β-decay branchings of the ^{69}Ni mother into the various levels of ^{69}Cu have been relied upon to postulate for ^{69}Ni a $(9/2^+)$ ground state [12]. Consequently, we can calculate $\log ft$ values assuming the absence of β feeding towards the daughter ground state.

In Fig. 6 we display the systematics of the odd $^{57-67}$Cu isotopes. A low-lying $1/2^-$ state is distinguished in each of these, for which the corresponding level in ^{69}Cu has been reported at 1096 keV [36]. The $5/2^-$ level appears in ^{69}Cu at 1214 keV [35]. The lower limit for the $\log ft$ value of 5.8 suggests the existence of additional high-energy γ rays that have escaped detection. The level at 2183 keV has been interpreted as the $9/2^-$ member of a collective band built on the $7/2^-$ state at 1712 keV [16].

The four levels at 2553, 2697, 2757, and 2802 keV are strongly fed with lower limits for the $\log ft$ values of 4.9, 4.3, 4.2, and 5.0. From the γ-ray deexcitation patterns, spin and parity assignments of $9/2^+$, $7/2^+$, and $11/2^+$ have been deduced for the first three of these [15]. Also for the level at 2802 keV a positive parity can be concluded. The level at 2603 keV may represent a $9/2^-$ state predicted by the empirical shell model at 2729 keV [16]. Since the shell model

does not account for additional levels below 1.5 MeV, it is unlikely that the order of the experimentally observed 154.1- and 1389.5-keV transitions is to be reversed.

In a recent experiment on ^{69}Co, a β-decaying isomer in ^{69}Ni has been detected [4]. Located at an excitation energy of 321 keV, a spin and parity of $1/2^-$ is assigned to this state [1]. Allowed Gamow-Teller decay feeds into the 1298 keV level in ^{69}Cu with a spin and parity of $3/2^-$, also present in the current data. A lower limit for the production of the isomer in this work is set to 0.74 at/μC, which amounts to nearly 20% of the production of ^{69}Ni.

B. ^{71}Cu

The β-decay scheme of ^{71}Ni is shown in Fig. 7. Complementary information is available from the discovery of a microsecond isomer in ^{71}Cu [1,3]. This $19/2^-$ state at 2756 keV is seen to decay through the 2129-, 1787-, 1190-, and 534-keV levels, with a weak indication for the 981-keV level. The energy determination for these states deviates at most 1 keV from our values.

Grzywacz *et al.* insert a 471-keV transition at the top of the level scheme [1], which Ishii *et al.* have thrown doubt upon [3]. Our placement of the 472.0(1) keV in the lower half of the diagram may offer a possible solution. Because of the closely matching intensities of the 161.4(1) keV with $\dagger_\gamma = 3.0(6)$ and the 744.7(1) keV with $\dagger_\gamma = 2.3(6)$, we cannot reliably ascertain the mutual order of these two lines. The level at 2290 keV therefore remains tentative.

Since the β decay of ^{71}Cu directly feeds 1/2 and 5/2 levels in ^{71}Zn, a $3/2^-$ assignment for the ground state is favored [12]. Assuming that a $(9/2^+)$ spin and parity for the ground state of the nickel mother nucleus is maintained, we conclude that no significant ground-state β branch in the decay of ^{71}Ni towards ^{71}Cu will be present.

The discovery of the $19/2^-$ microsecond isomer at 2756 keV establishes an $E2$ cascade to the ground state [1,3]. A spin and parity of $7/2^-$ for the level at 1190 keV and $11/2^-$ for the level at 2129 keV follow. Ishii *et al.* have suggested a $9/2^+$ signature for the state at 1787 keV [3], which, however,
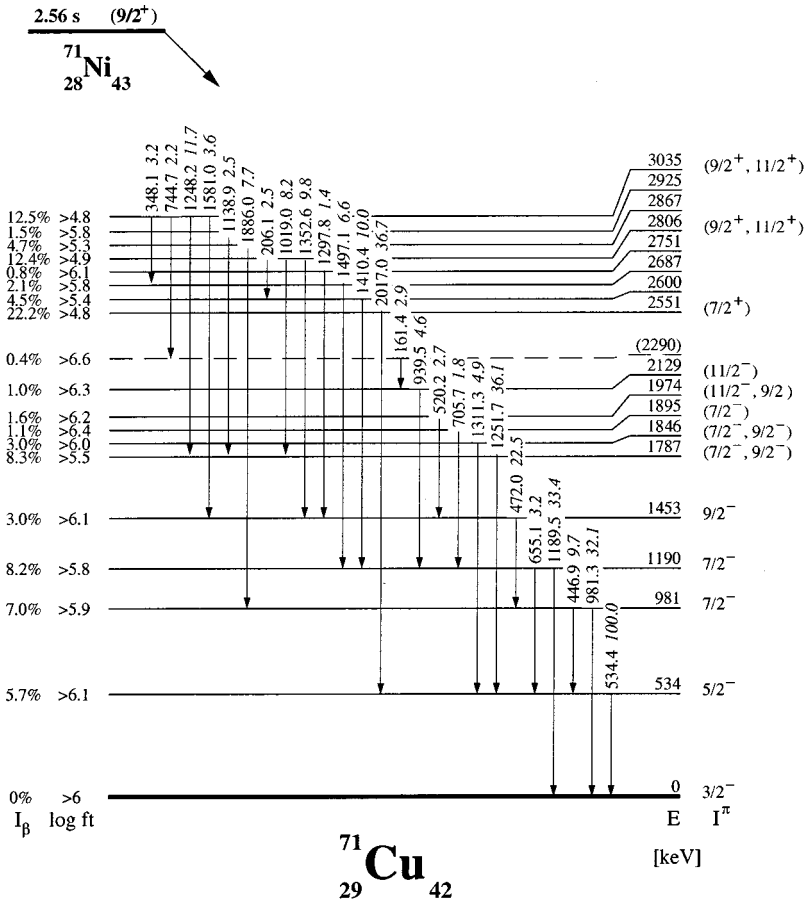
FIG. 7. Decay scheme of ^{71}Ni. For discussion, see text.

in Sec. VII we shall show to be questionable. We remind the reader that the apparently strong β branch to the 1787-keV state with a lower limit for the $\log ft$ value of 5.5 might be artificially induced by unresolved γ feeding from high-lying levels.

From Fig. 7 we see that for the three levels at 2551, 2806, and 3035 keV we compute respective lower limits for the $\log ft$ values of 4.8, 4.9, and 4.8. With this the structure bears resemblance to the set of positive-parity states that appears at approximately the same energy in ^{69}Cu.

Unlike ^{69}Ni, no long-lived low-spin isomer has been found in ^{71}Ni. However, it is possible that the β decay of this eventual $1/2^-$ isomer directly proceeds to the ^{71}Cu ground state, in which case it would not be detected by γ spectroscopy. Alternatively, according to shell-model calculations [9] it may not undergo β decay but instead deexcite through an $E3$ transition to a low-lying $7/2^+$ three-quasineutron state within ^{71}Ni.

C. ^{73}Cu

The level scheme of ^{73}Cu is depicted in Fig. 8. The placement of the 1708-keV state is rather arbitrary since the 676.9(7)- and 1542.2(8)-keV transitions both display an intensity of $\dagger_\gamma = 5(1)$. If their order would be inverted, a level at 843 keV would result. The limited statistics only allow one to quote upper limits for the β-decay intensities.

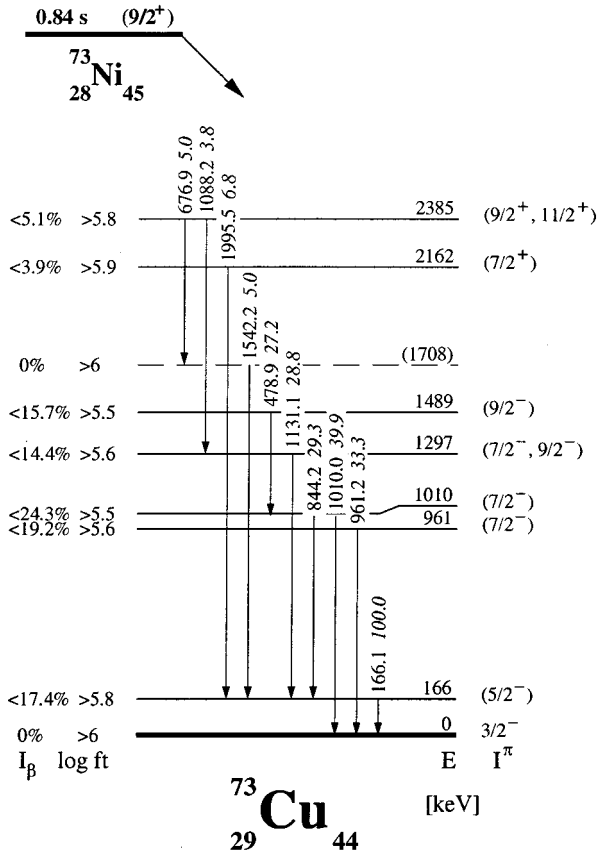The detection of considerable β feeding with a $\log ft$ of 5.4 in the decay of ^{73}Cu towards the $1/2^-$ ground state of ^{73}Zn argues for a $3/2^-$ assignment for the ground state of ^{73}Cu [21]. Adopting a $(9/2^+)$ ground-state spin and parity for ^{73}Ni, ground-state β feeding in the decay of ^{73}Ni to ^{73}Cu can be disregarded.

Analogous to the feeding pattern in ^{69,71}Cu, the levels at 2162 and 2385 keV may carry a positive parity. As a result of the rather faint statistics, several transitions with a relative intensity of $\dagger_\gamma \approx 10$ originating from fairly populated levels at 2–3 MeV might have been missed.

VII. DISCUSSION

In the following discussion leading configurations will be given with reference to the $N=40$ subshell, with the Fermi level situated between the neutron $p_{1/2}$ and $g_{9/2}$ orbitals. This is in the spirit of the work by other authors [16] but does not imply a $N=40$ shell closure.

We have performed shell-model calculations in the full $f_{5/2}$, $p_{3/2}$, $p_{1/2}$, and $g_{9/2}$ model space for both protons and neutrons. A realistic interaction derived from a G matrix was used [37]. Single-particle energies extracted from experimental data in ^{56}Ni and its neighbors ^{57}Ni and ^{57}Cu were modified in order to reproduce the spectroscopy of the Ni and Cu isotopes around $N=40$. Further details are given in Refs. [5,9]. Hereafter referred to as S3V$'$, the updated interaction yields the level schemes of Fig. 9. For reasons of simplicity we plot only the lowest $3/2^-$, $5/2^-$, $7/2^-$, and $9/2^-$ negative-parity states and the lowest $7/2^+$, $9/2^+$, and $11/2^+$ positive-parity states.
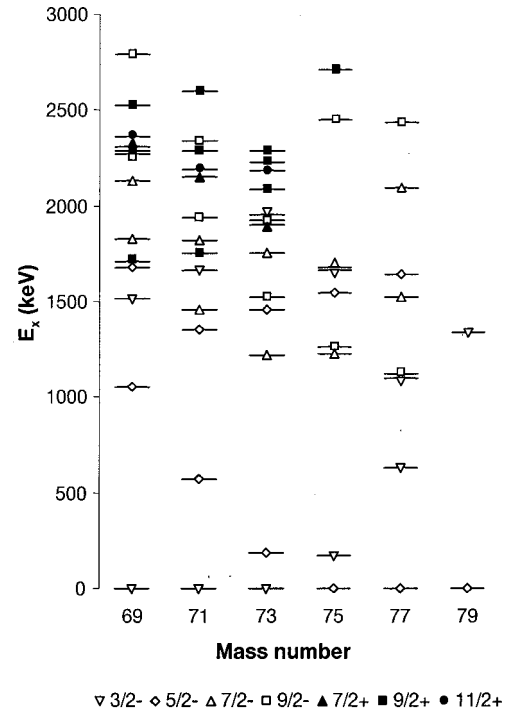
FIG. 8. Decay scheme of ^{73}Ni. For discussion, see text.

FIG. 9. Selected levels for $^{69-79}$Cu calculated with the S3V$'$ interaction.

In general, the results that have been reported in the literature assuming pure configurations and an empirical interaction [16] are in line with full shell-model calculations with a realistic interaction, except that there is no significant energy gap at $N=40$. Nevertheless, because of the transition from negative- to positive-parity orbitals, ^{68}Ni can still be considered as a reasonably stiff core. The calculations also indicate that any two-particle–two-hole ($2p2h$) neutron excitation is not of pure $\nu p_{1/2}^{-2}\ \nu g_{9/2}^2$ origin but highly mixed with or even dominated by the $\nu f_{5/2}^{-2}\ \nu g_{9/2}^2$ configuration.

A. ^{69}Cu

The shell model explains the $3/2^-$ spin and parity of the ground state of ^{69}Cu by a dominating $\pi p_{3/2}\nu p_{1/2}^2$ wave function component. The ($9/2^+$) ground state of the ^{69}Ni mother is understood as an uncoupled $g_{9/2}$ neutron. The most viable decay pattern of ^{69}Ni is the Gamow-Teller conversion of a $p_{1/2}$ neutron to a $p_{3/2}$ proton. This process may create the $\pi p_{3/2}(\nu p_{1/2}^{-1}\nu g_{9/2})_{5^-}$ and $\pi p_{3/2}(\nu p_{1/2}^{-1}\nu g_{9/2})_{4^-}$ multiplets. The former of these is equivalent to the coupling of the $p_{3/2}$ proton to the 5^- isomer in ^{68}Ni at 2847 keV, while the latter would reflect a 4^- state in ^{68}Ni that has not yet been identified but predicted to be situated 300 keV upwards [14].

The spin and parity for the lower quadruplet ranges from $7/2^+$ to $13/2^+$. The $13/2^+$ state, however, will not be populated in our work because of the selection rules for allowed β decay. It is otherwise known from transfer [15,16] and fragmentation experiments [1] and constitutes a microsecond iso-

mer at 2742 keV. The well-fed levels at 2553, 2697, and 2757 keV likely belong to the set of positive-parity states anticipated. Indeed, $9/2^+$, $7/2^+$, and $11/2^+$ assignments have been derived for the states at 2553, 2697, and 2757 keV [15]. The level at 2802 keV could be the $9/2^+$ member of the $\pi p_{3/2}(\nu p_{1/2}^{-1}\nu g_{9/2})_{4^-}$ multiplet, an assignment that would be compatible with the decay scheme.

The $1/2^-$ state at 1096 keV, reported in Fig. 6, can be connected with the $\pi p_{1/2}$ particle excitation and is not accessed by the β decay. The $5/2^-$ level at 1214 keV can be largely assigned to the $\pi f_{5/2}$ structure. The $7/2^-$ level at 1712 keV contains a major fraction of the $\pi f_{7/2}$ proton-hole strength, while the state at 2183 keV is seen as the $9/2^-$ member of a collective band built on this excitation [16]. The $7/2^-$ level at 1872 keV predominantly reflects the $\pi p_{3/2}(\nu p_{1/2}^{-2}\nu g_{9/2}^2)_{2^+}$ coupling, the three particles of which also would give rise to the ($9/2^-$) level at 2603 keV [16]. The $1/2^-$ β-decaying isomer at 321 keV in ^{69}Ni mentioned above likely corresponds to the $\nu p_{1/2}^{-1}\nu g_{9/2}^2$ configuration and decays to the 1298-keV level with spin and parity $3/2^-$ in ^{69}Cu, interpreted as a $\pi p_{3/2}\nu p_{1/2}^{-2}\nu g_{9/2}^2$ structure. The energy of this state nicely matches the calculated value of 1280 keV [16].

The S3V$'$ shell-model calculations described above account very well for the given interpretation. The relevant levels are shown in the leftmost column of Fig. 9. The lowest calculated $9/2^+$ state, which is for 77% dominated by the $\pi g_{9/2}$ component, is not fed by the β decay nor by the γ deexcitation of the $13/2^+$ isomer. This is due, respectively, to the isospin selection rule and the configuration hindrance for the $\pi p_{3/2}(\nu p_{1/2}^{-1}\nu g_{9/2})_{5^-}\rightarrow \pi g_{9/2}$ transition. The position of the $9/2_{2,3}^+$ states compares well to that of the experimentally

observed $(9/2^+)$ levels, although the calculated wave function of the $9/2_2^+$ state contains the $\pi p_{3/2} \nu f_{5/2}^{-1} \nu g_{9/2}$ rather than the $\pi p_{3/2} \nu p_{1/2}^{-1} \nu g_{9/2}$ structure, while the $9/2_3^+$ level would be highly mixed.

All negative-parity states except for the lowest $7/2^-$ level are well reproduced, which corroborates the assignment of the latter state to a 1p1h excitation from the $\pi f_{7/2}$ shell [16]. An analogous conclusion for the lowest $9/2^-$ state, however, is not supported by the realistic shell-model calculation.

B. ^{71}Cu

Moving from ^{69}Cu to ^{71}Cu involves the addition of one pair of neutrons to the $g_{9/2}$ orbital. The $3/2^-$ ground state of ^{71}Cu would still contain a major $\pi p_{3/2} \nu g_{9/2}^2$ component. Similar to ^{69}Ni, the $(9/2^+)$ mother nucleus would preferentially convert a $p_{1/2}$ neutron into a $p_{3/2}$ proton. The Gamow-Teller operation then produces the $\pi p_{3/2} (\nu p_{1/2}^{-1} \nu g_{9/2}^3)_{5^-}$ combination, generating a set of strongly populated positive-parity states that we expect to come across around 2.5–3 MeV. Coupling of the $p_{3/2}$ proton to the $(\nu p_{1/2}^{-1} \nu g_{9/2}^3)_{4^-}$ configuration, which shell-model calculations put 300 keV higher than the 5^- counterpart [14], would create additional levels around 3 MeV. The excited 2^+ states in ^{70}Ni, which are situated at 1259 keV [1] and 1868 keV [38], would give rise to weakly coupled particle-core levels near 1 to 2 MeV.

In view of the general good agreement between calculations and experiment, it should be noted that it is difficult to find in the shell-model results an appropriate candidate for the 2_2^+ state in ^{70}Ni. Therefore this could well be a proton core-excited state, which is excluded from the shell-model space.

Since multiparticle excitations cannot account for the first excited state at 534 keV in ^{71}Cu and given the fact that the level is not bypassed in the β decay of ^{71}Ni towards the $3/2^-$ ground state of ^{71}Cu, the state at 534 keV can only be explained as resulting from the $\pi f_{5/2}$ single-particle excitation. The lower limit for the log ft value of 6.1 indicates that part of the feeding to this level by high-energy γ rays might have been missed. Comparing the position of this $5/2^-$ level in ^{71}Cu to that in the odd $^{57-69}$Cu isotopes from Fig. 6, one ascertains a sudden steep drop. The assessment becomes especially intriguing if one realizes that for all preceding isotopes the energy of this state remains rather constant around 1 MeV.

Calculations by Oros-Peusquens and Mantica within the particle-core coupling model (PCM) have identified the state at 981 keV as the $f_{7/2}^{-1}$ proton hole, onto which a quasiband is residing in the same manner as for ^{69}Cu [39]. The levels at 981, 1453, and 1974 keV would belong to this structure and hence would show a spin and parity of $7/2^-$, $9/2^-$, and $11/2^-$, respectively. However, as Grzywacz et al. observed the 472.0- and 981.3-keV rays, but not the 520.2-keV line [1], it is possible that the 1974-keV level does not correspond to the $11/2^-$ yrast state but instead to any other adjacent 9/2 structure built on the $\pi f_{7/2}^{-1}$ hole.

The states at 1190 and 2129 keV with respective spin and parity of $7/2^-$ and $11/2^-$ are part of the $E2$ sequence deexciting the $19/2^-$ microsecond isomer at 2756 keV. The isomer is explained as the coupling of the $p_{3/2}$ proton to the 8^+ isomer in ^{70}Ni that is seen at a comparable energy of 2860 keV [1,15]. In both nuclei, the $E2$ cascade runs down the $\nu g_{9/2}^2$ seniority scheme, which is well accounted for in the shell-model calculations [9].

Both levels at 1787 and 1846 keV decay to the $\pi f_{5/2}$ level at 534 keV. Since the first excited 2^+ state in ^{70}Ni is found at 1259 keV [1], they may result from the $2_1^+ (^{70}\text{Ni}) \otimes \pi f_{5/2}$ configuration. The β decay would populate the $7/2^-$ and $9/2^-$ components; however, the mutual assignment would not be established unambiguously. Note that this interpretation would contradict the $9/2^+$ signature for the 1787-keV level suggested by Ishii et al. [3]. In fact, the latter seems untenable as the decay of the $9/2^+$ state would bypass the available $7/2^-$ and $9/2^-$ levels. Note that although the S3V′ model predicts a level with a major $\pi g_{9/2}$ component at 1755 keV, population of this excitation would be unlikely because of configuration hindrance. The lowest $9/2^-$ level is calculated at 200 keV higher.

Coupling of the second 2^+ state in ^{70}Ni at 1868 keV [38] to the $p_{3/2}$ proton creates a $7/2^-$ multiplet member, which is accessible by the β decay. The observed level at 1895 keV constitutes a valid candidate for this structure. The three levels at 2551, 2806, and 3035 keV likely correspond to the $\pi p_{3/2} (\nu p_{1/2}^{-1} \nu g_{9/2}^3)_{5^-}$ multiplet, which thus appears at approximately the same energy as in ^{69}Cu. From these states only the 2551-keV level connects to the $5/2^-$ excitation at 534 keV, indicating a spin and parity of $7/2^+$. For the states at 2806 and 3035 keV, we cannot discriminate between a spin and parity of $9/2^+$ or $11/2^+$. The remaining levels at 2600, 2687, 2751, 2867, and 2925 keV may arise from the $\pi p_{3/2} (\nu p_{1/2}^{-1} \nu g_{9/2}^3)_{4^-}$ or $4^+ (^{70}\text{Ni}) \otimes \pi f_{5/2}$ couplings.

C. ^{73}Cu

The $3/2^-$ assignment for the ground state of ^{73}Cu is understood from the $\pi p_{3/2} \nu g_{9/2}^4$ configuration. From an analogous reasoning as developed for ^{71}Cu, the first excited state at 166 keV is most likely produced by the $\pi f_{5/2}$ configuration. Hence we suggest for this level a $5/2^-$ spin and parity. Looking at Fig. 6, one appreciates a striking steepness in the downwards trend of the excitation energy of this orbital.

As a result of the PCM calculations by Oros-Peusquens and Mantica, the level at 961 keV has tentatively been interpreted as the $2_1^+ (^{72}\text{Ni}) \otimes \pi p_{3/2}$ configuration with spin and parity $7/2^-$ and the state at 1010 keV cautiously as the $\pi f_{7/2}^{-1}$ hole excitation, equally with spin and parity $7/2^-$ [39]. Like in the case of ^{69,71}Cu, the shell model accounts for only one $7/2^-$ state at this energy, supporting the $\pi f_{7/2}^{-1}$ assignment for the other. We suggest furthermore that the 1297-keV excitation corresponds to the $2_1^+ (^{72}\text{Ni}) \otimes \pi f_{5/2}$ coupling with spin and parity $7/2^-$ or $9/2^-$. The level at 1489 keV may belong to a quasiband, built on the $\pi f_{7/2}^{-1}$ intruder in a similar manner as for ^{69,71}Cu and resulting in a $9/2^-$ assignment. On the other hand, from Fig. 9 one reads that the shell model does reproduce $9/2^-$ states at this energy.

The level at 2162 keV could represent the $7/2^+$ member of the $\pi p_{3/2}(\nu p_{1/2}^{-1} \nu g_{9/2}^5)_{5^-}$ multiplet, created by the Gamow-Teller decay of an inner $p_{1/2}$ neutron in ^{73}Ni. Alike the γ pattern in ^{69,71}Cu, it decays directly to the first excited state at 166 keV. The 2385-keV excitation might as well belong to this multiplet and carry a spin and parity of $9/2^+$ or $11/2^+$. The shell model calculates the $\pi g_{9/2}$ single-particle state at 2088 keV, but this structure might not be accessible due to configuration hindrance.

D. Monopole migration

The existence of systematic energy shifts of specific single-particle levels has been pointed out by various authors [9,40,41]. Known as monopole migration, it has been traced back to the first term in the multipole expansion of the residual proton-neutron interaction. A clear illustration of the effect is provided in the evolution of the level structure between ^{91}Zr and ^{101}Sn. For that region the $\pi g_{9/2}$ orbital is gradually filled, while at the same time the energy of the $\nu g_{7/2}$ configuration sharply drops with respect to all other single-particle neutron states of the $50 < N < 82$ neutron shell. Other examples of monopole migration exist for the Sb isotopes, where the $\pi g_{7/2}$ state descends with a growing occupancy of the $\nu h_{11/2}$ orbital, and for the $N = 83$ isotones, where the $\nu h_{9/2}$ excitation energy decreases as the $\pi h_{11/2}$ state is populated.

With respect to the $^{57-73}$Cu isotopes, the $3/2^-$ ground state is primarily defined by the $\pi p_{3/2}$ configuration. For $^{57-69}$Cu the position of the first $5/2^-$ level, attributed to the $\pi f_{5/2}$ orbital, remains rather immobile at 1 MeV. However, simultaneously with the filling of the $\nu g_{9/2}$ neutron orbital, the gap between the $\pi p_{3/2}$ and $\pi f_{5/2}$ levels rapidly decreases.

The drift of shell-model orbitals is also supported by theory. In Fig. 6 the predicted single-particle levels are drawn for ^{79}Cu. They stem from two different sets of calculations for the $N = 50$ isotones. The work by Ji and Wildenthal (JW) adds protons to a ^{78}Ni core [42], the model by Sinatkas, Skouras, Strottman, and Vergados (S3V) introduces proton holes into ^{100}Sn [37]. Both groups manage to reproduce the known structures in the intermediate nuclei from ^{78}Ni to ^{100}Sn only if they fix the $\pi f_{5/2}$ orbital in ^{79}Cu far below the $\pi p_{3/2}$ state. Especially the $3/2^-$ ground states observed for ^{85}Br and ^{87}Rb imply that for these nuclei the $\pi f_{5/2}$ orbital is already completely filled and is situated below the $\pi p_{3/2}$ level.

Also in the realistic shell-model calculations the monopole shift is naturally reproduced. In earlier publications this has been demonstrated for the $N = 51$ isotones beyond ^{91}Zr [9], while for ^{71,73}Cu it is illustrated in Fig. 9. Besides the behavior of the first excited state also the calculated energy of the $7/2^+$, $9/2^+$, and $11/2^+$ levels in $^{69-73}$Cu is close to the experimentally observed values. As aforementioned the $\pi g_{9/2}$ single-particle state may not be populated easily in β decay by a non-spin-flip transition or in the subsequent γ decay due to configuration hindrance. Furthermore, the S3V′ results do not account for the $7/2^-$ levels at 981 keV in ^{71}Cu and 1010 keV in ^{73}Cu. This supports the interpretation that these correspond to the $\pi f_{7/2}^{-1}$ hole excitation, which indeed is not included in the shell-model space.

Alternatively, Oros-Peusquens and Mantica have applied a PCM approach, which enables the extraction of the pure single-particle energies from the experimental data by correcting for the quadrupole and octupole terms in the particle-vibration interaction [39]. From the analysis the authors conclude that the single-particle energy of the $\pi f_{5/2}$ orbital would reside 2 MeV below the $\pi p_{3/2}$ state in ^{78}Ni. However, if the available ground-state data for ^{73}Cu would not have been taken into account in the PCM, the theory would have predicted an exceptionally low excitation energy for the $\pi f_{7/2}$ configuration in the latter nucleus, which possibly would even supplant the ground state. Moreover, it is argued that the states at 2553 keV in ^{69}Cu, 1787 keV in ^{71}Cu, and 1297 or 1489 keV in ^{73}Cu all contain a dominant $\pi 1 g_{9/2}$ component. In the energy decrease of this presumed structure a manifestation of monopole migration is discerned.

Contrary to the PCM, the lowest $9/2^+$ state given by the S3V′ model rises in energy from 1.7 MeV in ^{69}Cu to 2.7 MeV in ^{75}Cu and further to 3.6 MeV in ^{79}Cu. In addition, as discussed above the $\pi g_{9/2}$ single-particle state cannot be established amongst the states that have been observed experimentally. For a possible explanation, we recall that the monopole effect Δ_M is proportional to the average interaction energy in a multiplet,

$$\Delta_M \propto \frac{\sum (2J+1)\langle j_1 j_2 | V | j_1 j_2 \rangle_J}{\sum (2J+1)},$$

with j_1 the proton spin, j_2 the neutron spin, J the multiplet spin, and V the potential. Because the highest spin values are weighted most, they account for most of the monopole energy, provided there is a good overlap of the respective radial wave functions. Further, for identical orbitals where $j_1 = j_2$ the proton-neutron interaction alternates between $T = 0$ and $T = 1$, according to $J + T =$ odd. In the effective interaction of Gross and Frenkel [43] the $\langle gg | V | gg \rangle_{T=1}$ matrix elements are repulsive for $J > 4$, while all others are binding. Therefore there would be a deficiency of binding for the $\pi g_{9/2} \nu g_{9/2}$ orbitals, which could explain a smaller monopole effect than anticipated.

VIII. CONCLUSIONS

As a result of the unique integration at LISOL of resonant laser ionization with ion guidance, it has been possible to develop an ion source that combines fast extraction, selectivity, and efficiency. The source has been configured for proton-induced fission of ^{238}U, which has led to the production of the neutron-rich $^{68-74}$Ni isotopes and the first observation of γ lines following the β decay of $^{70-74}$Ni.

Half-lives have been determined for $^{68-74}$Ni. Cross sections have been deduced, covering a range for over two orders of magnitude. The mean of the distribution is situated at mass 69.4(3), which is about 1 mass unit closer to stability than predicted by Huhta *et al.* [30]. An extrapolation of the yield curve results in an estimated cross section for ^{78}Ni of

10 pb. A production rate of 0.3 atoms per day can be foreseen with the current setup at LISOL, which is comparable with other production mechanisms.

Level schemes have been constructed for ^{69,71,73}Cu. The decay of a $p_{1/2}$ neutron into a $p_{3/2}$ proton strongly feeds a $7/2^+$, $9/2^+$, $11/2^+$ multiplet in the odd ^{69,71}Cu isotopes, probably also existing in ^{73}Cu but not unambiguously established. Of particular interest is the sharp drop of the $\pi f_{5/2}$ excitation in these nuclides relative to the $\pi p_{3/2}$ ground state. Known as monopole migration, the energy shift originates from the residual proton-neutron interaction, while its mag-nitude is proportional to the overlap of the proton and neutron wave functions. Realistic shell-model calculations satisfactorily account for the observed behavior, but partially deny results obtained by the particle-core coupling model.

[1] R. Grzywacz et al., Phys. Rev. Lett. **81**, 766 (1998).

[2] S. Franchoo et al., Phys. Rev. Lett. **81**, 3100 (1998).

[3] T. Ishii, M. Asai, I. Hossain, P. Kleinheinz, M. Ogawa, A. Makishima, S. Ichikawa, M. Itoh, M. Ishii, and J. Blomqvist, Phys. Rev. Lett. **81**, 4100 (1998).

[4] W.F. Mueller et al., Phys. Rev. Lett. **83**, 3613 (1999).

[5] J.M. Daugas et al., Phys. Lett. B **476**, 213 (2000).

[6] J. Dobaczewski, I. Hamamoto, W. Nazarewicz, and J. Sheikh, Phys. Rev. Lett. **72**, 981 (1994).

[7] J. Zylicz, J. Dobaczewski, and Z. Szymański, in ENAM 98, *Exotic Nuclei and Atomic Masses*, edited by B. Sherrill, D. Morrissey, and C. Davids, AIP Conf. Proc. No. 455 (AIP, Woodbury, NY, 1998), p. 813.

[8] J. Engel, M. Bender, J. Dobaczewski, W. Nazarewicz, and R. Surman, Phys. Rev. C **60**, 014302 (1999).

[9] H. Grawe et al., in *Proceedings of the Workshop on The Beta Decay, from Weak Interaction to Nuclear Structure*, Strasbourg, 1999, edited by P. Dessagne, A. Michalon, and C. Miehé (Ires, Strasbourg, 1999), p. 211.

[10] K.-L. Kratz, J.-P. Bitouzet, F.-K. Thielemann, P. Möller, and B. Pfeiffer, Astrophys. J. **403**, 216 (1993).

[11] W.-D. Schmidt-Ott et al., in *Nuclei Far from Stability*, edited by I. Towner AIP Conf. Proc. No. 164 (AIP, Woodbury, NY, 1988), p. 365.

[12] U. Bosch et al., Nucl. Phys. **A477**, 89 (1988).

[13] M. Bernas, P. Dessagne, M. Langevin, J. Payet, F. Pougheon, and P. Roussel, Phys. Lett. **113B**, 279 (1982).

[14] R. Broda et al., Phys. Rev. Lett. **74**, 868 (1995).

[15] R. Broda et al., in *Proceedings of the International Conference on Fission and Properties of Neutron-Rich Nuclei*, Sanibel Island, 1997, edited by J. Hamilton and A. Ramayya (World Scientific, Singapore, 1998), p. 202.

[16] T. Ishii, M. Asai, A. Makishima, I. Hossain, M. Ogawa, J. Hasegawa, M. Matsuda, and S. Ichikawa, Phys. Rev. Lett. **84**, 39 (2000).

[17] R. Kirchner, Nucl. Instrum. Methods Phys. Res. B **26**, 204 (1987).

[18] A. Jokinen et al., Nucl. Instrum. Methods Phys. Res. B **126**, 95 (1997).

[19] M. Bernas, P. Armbruster, J. Bocquet, R. Brissot, H. Faust, C. Kozhuharov, and J. Sida, Z. Phys. A **336**, 41 (1990).

[20] F. Ameil et al., Eur. Phys. J. A **1**, 275 (1998).

[21] M. Huhta, P. Mantica, D. Anthony, P. Lofy, J. Prisciandaro, R. Ronningen, M. Steiner, and W.B. Walters, Phys. Rev. C **58**, 3187 (1998).

[22] J. Prisciandaro, P. Mantica, A. Oros-Peusquens, D. Anthony, M. Huhta, P. Lofy, and R. Ronningen, Phys. Rev. C **60**, 054307 (1999).

[23] C. Engelmann et al., Z. Phys. A **352**, 351 (1995).

[24] Y. Kudryavtsev et al., Nucl. Instrum. Methods Phys. Res. B **114**, 350 (1996).

[25] P. Van den Bergh et al., Nucl. Instrum. Methods Phys. Res. B **126**, 194 (1997).

[26] GEANT, Detector Description and Simulation Tool, Cern, Geneva, 1993.

[27] L. Vermeeren et al., Nucl. Instrum. Methods Phys. Res. B **126**, 81 (1997).

[28] R. Firestone, *Table of Isotopes*, 8th ed. (Wiley, New York, 1996).

[29] B. Fogelberg (private communication).

[30] M. Huhta et al., Phys. Lett. B **405**, 230 (1997).

[31] J. Benlliure, A. Grewe, M. de Jong, K.-H. Schmidt, and S. Zhdanov, Nucl. Phys. **A628**, 458 (1998).

[32] I. Reusen et al., Phys. Rev. C **59**, 2416 (1999).

[33] D. Habs et al., Prog. Part. Nucl. Phys. **38**, 111 (1997).

[34] G. Audi, O. Bersillon, J. Blachot, and A. Wapstra, Nucl. Phys. **A624**, 1 (1997).

[35] B. Zeidman and J. Nolen, Jr., Phys. Rev. C **18**, 2122 (1978).

[36] F. Ajzenberg-Selove, R. Brown, E. Flynn, and J. Sunier, Phys. Rev. C **24**, 1762 (1981).

[37] J. Sinatkas, L. Skouras, D. Strottman, and J. Vergados, J. Phys. G **18**, 1377 (1992).

[38] W.F. Mueller et al., Phys. Rev. C **61**, 054308 (2000).

[39] A. Oros-Peusquens and P. Mantica, Nucl. Phys. **A669**, 81 (2000).

[40] K. Heyde, J. Jolie, J. Moreau, J. Ryckebusch, M. Waroquier, P. Van Duppen, M. Huyse, and J. Wood, Nucl. Phys. **A466**, 189 (1987).

[41] W.B. Walters, in *Nuclear Fission and Fission-Product Spectroscopy*, edited by Gabriele Fioni et al., AIP Conf. Proc. No. 447 (AIP, Woodbury, NY, 1998), p. 196.

[42] X. Ji and B. Wildenthal, Phys. Rev. C **40**, 389 (1989).

[43] R. Gross and A. Frenkel, Nucl. Phys. **A267**, 85 (1976).